2022 European Control Conference (ECC)
July 12-15, 2022. London, United Kingdom

An Adaptive Time-Headway Policy for Lower Energy Consumption in Autonomous Vehicle Platoons

Rohith G.* , K. B. Devika†, Prathyush P. Menon* and Shankar C. Subramanian†
*College of Engineering, Mathematics and Physical Sciences,
University of Exeter, Exeter, EX4 4QF, United Kingdom.
Email: rohith044@gmail.com
†Department of Engineering Design,
Indian Institute of Technology Madras, Chennai, 600036, India.

Abstract— **Road vehicle platoons improve fuel economy by limiting the aerodynamic drag. Time-headway along with operating speed dictates the intervehicular spacing, and hence the aerodynamic drag reduction. This paper proposes an adaptive scheme to adjust the magnitude of time-headway to reduce energy consumption according to operating speed. An 'energy consumption - time-headway - speed map' is generated using a complete vehicle dynamics-based platoon framework integrated with a sliding mode controller. This map could be used to adaptively adjust time-headway for an expected energy consumption magnitude and to predict the energy consumed for the completion of a route. Constraints are enforced limiting the time-headway values to meet deceleration demand. The proposed approach was found to result in an energy consumption reduction up to 35% compared to conventional approaches where the time-headway values are kept constant.**

Keywords: Autonomous platoon, deceleration demand, energy consumption, sliding mode controller, time-headway

I. Introduction

Autonomous/semi-autonomous truck platoons are regarded as a potential fuel-efficient and green solution to meet the ever-increasing freight transportation demand [1], [2]. In a platoon formation, vehicles operate close to each other with minimum possible spacing between one another. This reduces aerodynamic drag associated with individual vehicles, a major contributor to fuel consumption, especially at high operating speeds. This advantage can be utilised to reduce energy consumption, especially during highway operations. In addition to using fully autonomous platoons, this idea could be extended to human-operated platoons by providing autonomy during cruise mode, making them semi-autonomous. Apart from the attribute of being fuel-economical, an automated/semi-autonomous truck platoon would result in reduced operation cost, less human resource requirement, safer operations, reduced greenhouse gas emission, and effective road infrastructure utilisation [3], [4], [5].

Autonomous/semi-autonomous platoon operation demands controllers to maintain the desired speed and intervehicular spacing between the constituent vehicles. Moreover, these controllers should ensure platoon string stability in the event of any possible perturbation. A vehicle platoon is said to be string stable if the intervehicular spacing errors between consecutive vehicles are bounded uniformly in time, provided the initial spacing errors are bounded [6]. In this regard, this work utilises a sliding mode based control framework for ensuring autonomous and string stable platoon operation.

It is always convenient to define a desired value for the intervehicular spacing considering stability requirements. Usually, this desired value is either chosen as a constant, resulting in a constant spacing policy [7] or as a function of vehicle speed and the temporal spacing between two consecutive vehicles, resulting in a constant time-headway policy (CTH) [8]. In the CTH policy, the time-headway is kept constant. Also, as speed increases, the intervehicular spacing increases, contributing to high aerodynamic drag and consequently increased energy consumption. To address this issue, an adaptive time-headway policy is proposed in this work.

Since the total energy consumption is a function of vehicle speed and time-headway, a map characterising energy consumption as a function of these two parameters is generated using a vehicle dynamics-based nonlinear platoon framework. Using this map, it is possible to select appropriate time-headway values corresponding to different operating speeds and desired energy consumption magnitudes. The map can also be used to predict the energy required for a specific route according to different operating conditions. As speed increases, the vehicles are brought closer to each other to reduce the aerodynamic drag for maintaining a desired energy consumption value. Further, the energy consumption map is suitably modified to incorporate deceleration demands. The proposed platoon framework with adaptive time-headway policy is shown in Fig. 1. The desired intervehicular spacing is computed based on the time-headway values generated by the energy consumption map. The controller instantaneously synthesises the drive/brake torque inputs to maintain the desired intervehicular spacing.

II. Platoon Model

A truck platoon framework with one leader and N identical followers has been considered in this work. The assumptions made in this study are:

- Only the longitudinal dynamics of the vehicle has been considered in the design.
- The parameters of the tyre model and vehicle are assumed to be known.

978-3-907144-06-0 ECC2022 (IEEE Xplore)

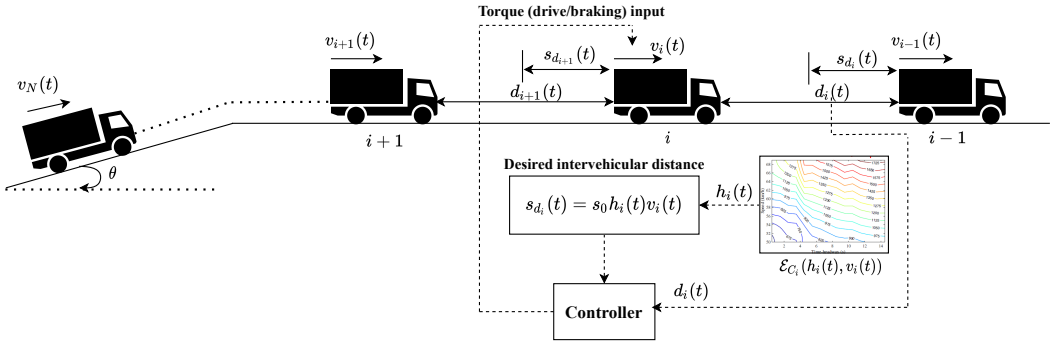

Fig. 1: Platoon framework with proposed adaptive time-headway approach.

- An equal load distribution on the left wheel and the right wheel of a specific axle of the vehicle is assumed.
- Each vehicle in the platoon has position and speed information of its immediate neighbours.

The kinematic equation that characterises the leader vehicle in the platoon is

$$\dot{x}_0(t) = v_0(t), \tag{1}$$

where, $x_0(t)$ and $v_0(t)$ are the position, and longitudinal speed of the leader vehicle, $v_0(t)$ is the speed to be tracked by the follower vehicles. As presented in [9], a complete vehicle dynamics model that incorporates factors such as resistive forces, wheel slip, tyre model, wheel dynamics, normal forces and actuator dynamics has been used in this paper to characterise the follower vehicles. The position and longitudinal speed dynamics of the i^{th} vehicle are represented as

$$\begin{aligned} \dot{x}_i(t) &= v_i(t), \\ \dot{v}_i(t) &= \Omega(v_i(t), \tau_{ji}(t)), \end{aligned} \tag{2}$$

where, $\tau_{ji}(t)$ represents the drive/brake input with $j = f, r$, indicating front and rear wheels, respectively. Here, $\Omega(v_i(t), \tau_{ji}(t))$ represents a nonlinear function in $v_i(t)$ and $\tau_{ji}(t)$, and is given by

$$\Omega(v_i(t), \tau_{ji}(t)) = \frac{1}{m_i}\left(\sum_{j=f,r} F_{xji}(\lambda_{ji}(t), \tau_{ji}(t)) - F_{Ri}(t)\right). \tag{3}$$

Here, m_i represents the mass of the i^{th} truck and $F_{xji}(\lambda_{ji}(t), \tau_{ji}(t))$ represents the longitudinal force at the tyre-road interface. The longitudinal force is a function of the longitudinal wheel slip ratio, $\lambda_{ji}(t)$, the friction coefficient (μ) between the tyre and the road, drive/brake input (τ_{ji}), and the normal load on the tyre ($F_{zji}(t)$) [10]. The slip ratio is given by

$$\lambda_{ji}(t) = \begin{cases} \frac{v_i(t) - R_i\ \omega_{ji}(t)}{v_i(t)}, & \text{during braking,} \\ \frac{R_i\ \omega_{ji}(t) - v_i(t)}{R_i\ \omega_{ji}(t)}, & \text{during drive,} \end{cases} \tag{4}$$

where, $\omega_{ji}(t)$ represents the angular speed of the wheels. Assuming equal load distribution between the left and right wheels of the same axle, the normal loads are

$$\begin{aligned} F_{zfi}(t) &= \frac{m_i(g(l_{ri}\cos\theta - h_i\sin\theta) - a_i(t)h_i) - F_{ai}(t)\ h_{ai}}{l_{fi} + l_{ri}}, \\ F_{zri}(t) &= \frac{m_i(g(l_{fi}\cos\theta + h_i\sin\theta) + a_i(t)h_i) + F_{ai}(t)\ h_{ai}}{l_{fi} + l_{ri}}, \end{aligned} \tag{5}$$

where, R_i is the tyre radius, and $a_i(t)$ represents the longitudinal acceleration. The height of the center of gravity (C.G.) of the vehicle is indicated by h_i, and h_{ai} represents the height of the location at which the resultant aerodynamic force acts. Here, l_{fi} and l_{ri} show the longitudinal distances of the front and rear axles from the C.G. of the vehicle, respectively, and θ represents the road gradient, which is defined to be positive for an upgrade and negative for a downgrade.

The wheel dynamics is given by,

$$\dot{\omega}_{ji}(t) = \frac{1}{I_{ji}}(\tau_{ji}(t) - R_i F_{xji}(\lambda_{ji}(t))), \tag{6}$$

where, ω_{ji} represent the angular speed of the wheels, and I_{ji} is the moment of inertia of wheels. In this study, the Magic Formula (MF) tyre model [11] has been used to characterise the longitudinal force at the tyre-road interface, which is given by

$$F_{xji}(\lambda_{ji}(t)) = D\sin(C\tan^{-1}(\Gamma - E(\Gamma - \tan^{-1}\Gamma))) + S_V, \tag{7}$$

where, $\Gamma = B\lambda_x(t)$, and $\lambda_x(t) = \lambda_{ji}(t) + S_H$. The MF model parameters, B, C, D, E, S_H, S_V were obtained from the vehicle dynamic simulation software, IPG TruckMaker®.

In Eq. (3), $F_{Ri}(t)$ represents the total resistive force due to rolling resistance, aerodynamic drag and road gradient on the i^{th} vehicle, which is given by

$$F_{Ri}(t) = -m_i g(f_i\cos\theta + \sin\theta) - \rho a_{fi} C_{Di}(t)\frac{v_i(t)^2}{2}, \tag{8}$$

where, f_i and ρ represent the rolling friction coefficient and the air density, respectively. The vehicle frontal area is represented by a_{fi} and C_{Di} indicates the drag coefficient.

The transfer function of the pneumatic brake system of a truck obtained via Hardware in Loop experimentation [12] is given by

$$P_{ji}(s) = \frac{\tau_{ji}(s)}{\tau_{desji}(s)} = \frac{1}{1 + \delta_{ji}s}e^{-T_{dji}s}, \tag{9}$$

where, δ_{ji} represents the time constant, and T_{dji} is the time delay, and τ_{desji} and τ_{ji} indicate the demanded brake torque and actual brake torque developed, respectively. The experimentally corroborated values for this model parameters are $\delta_{ji} = 260$ ms and $T_{dji} = 45$ ms [12], and have been utilized in this study. From literature, it was understood that a first-order model with time constant and delay is suitable for approximating the powertrain dynamics during the acceleration/drive phase [13]. Hence, a similar model as presented in Eq. (9) has been used to incorporate powertrain dynamics during the acceleration phase.

III. Energy Consumption as a Function of Intervehiclular Spacing

One of the major advantages of platooning is the improvement in fuel efficiency by reducing the aerodynamic drag [14], a significant contributor to the energy consumption associated with individual vehicles. The aerodynamic drag force for each vehicle in the platoon is given by

$$F_{ai}(t) = \rho\ a_{fi}\ C_{Di}(t)\frac{v_i(t)^2}{2}, \tag{10}$$

where, ρ is the density of air, $C_{Di}(t)$ is the aerodynamic drag coefficient and a_{fi} is the frontal area of the vehicle, which is assumed to be same for each vehicle ($a_{fi} = a_f$). The reduction in aerodynamic drag is attributed to how closely the vehicle are spaced from one another, defined as the intervehicular spacing, $d_i(t)$. The intervehicular spacing between a pair of vehicles in the platoon at each time instant t is given by

$$d_i(t) = x_{i-1}(t) - x_i(t), \tag{11}$$

where, $x_{i-1}(t)$ and $x_i(t)$ are the positions of the $(i-1)^{\text{th}}$ and i^{th} vehicle in the platoon. Since the platoon efficacy depends on the magnitude of $d_i(t)$ [9], it is important to maintain $d_i(t)$ at a particular desired magnitude. To achieve this, the desired inter-vehicular distance is defined as

$$s_{d_i}(t) = s_0 + h_i(t)v_i(t), \tag{12}$$

where, s_0 and $h_i(t)$ represent standstill spacing and the time-headway, respectively. Standstill spacing refers to the spacing between consecutive vehicles in the platoon when they are at rest. Time headway is defined as the time elapsed between the rear end of the preceding vehicle passing a point on the road to the time at which the front of the succeeding vehicle passes the same point.

The variation of aerodynamic drag in terms of $C_{Di}(t)$ as a function of $d_i(t)$ is given by [14],

$$C_{Di}(t) = C_{D0}(\gamma_1 d_i(t)^{\gamma_2} + \gamma_3). \tag{13}$$

Here, C_{D0} represent the drag coefficient of any individual vehicle (not operating in a platoon formation), and the parameters γ_1,γ_2, and γ_3 are obtained empirically [14].

During the drive mode, the total energy consumed can be written as

$$\mathcal{E}_{C_i} = \int_0^{T_t} \Big(F_{xfi}(t) + F_{xri}(t)\Big)v_i(t)dt, \tag{14}$$

where T_t is the total drive time.

IV. Controller Design for Autonomous Platoon Operation

In this work, the well-established sliding mode control (SMC) technique has been used to design the autonomous controller that could establish desired speed and spacing in the platoon. This controller has been designed to attenuate the spacing errors along the platoon leading to string stable operation.

From Section II, substituting for F_{xji} in Eq. (3) using Eq. (6), the individual vehicle dynamics in Eq. (2) can be presented as,

$$\begin{aligned}\dot{x}_i(t) =& v_i(t),\\ \dot{v}_i(t) =& \frac{1}{m_i}\Bigg[\frac{1}{R_i}(\tau_{fi}(t) - I_{fi}\dot{\omega}_{fi}(t)) + \frac{1}{R_i}(\tau_{ri}(t) - \\ & I_{ri}\dot{\omega}_{ri}(t)) - F_{Ri}(t)\Bigg].\end{aligned} \tag{15}$$

To design the SMC, the following function is defined [8]:

$$s_i(t) = e_i(t) + \int_0^t \kappa e_i(\tau)d\tau. \tag{16}$$

Let $e_i(t)$ represent the spacing error between two consecutive vehicles. It is given by

$$e_i(t) = d_i(t) - s_{d_i}(t), \tag{17}$$

The function presented in Eq. (16) is defined in such a way that it should drive the non-zero $e_i(t)$ (if any) to zero and track the desired speed. The function is selected in this form to avoid using the preceding vehicle jerk (derivative of acceleration) data.

It should be noted that driving $e_i(t)$ to zero might not be enough to ensure string stability. The spacing error propagation should also be considered and should be attenuated. To achieve this, the sliding function is redefined as,

$$S_i(t) = \begin{cases} qs_i(t) - s_{i+1}(t), & i = 1, ..., N-1 \\ qs_i(t), & i = N \end{cases}, \tag{18}$$

where, $0 < q < 1$.
To eliminate chattering issue in conventional SMC, the power rate exponential reaching law (PRERL) [15] is used in this work, which is given by

$$\dot{S}_i(t) = -K_{si}|S_i(t)|^{\chi}\text{sign}(S_i(t)). \tag{19}$$

Here $K_{si} = \frac{\psi}{\delta_0 + (1-\delta_0)e^{-\alpha|S_i(t)|^p}}$ [15]. Here, $\psi > 0$ is the controller gain, $\delta_0 < 1, \alpha > 0, 0 < \chi < 0.5$ and $p > 0$ are the controller design parameters.

On obtaining the first derivatives of equations (16) and (18), and using the vehicle dynamics equation (15), and the PRERL structure in equation (19), the control input, $\tau_{ri}(t)$ can be obtained. Assuming the vehicles are rear-wheel driven, during drive mode, $\tau_{fi}(t) = 0$, and $\frac{\tau_{fi}(t)}{\tau_{ri}(t)} = \frac{\beta}{1-\beta}$ during braking, assuming a linear brake torque proportion, β, with $\beta = 0.5$.

Based on this, during the drive mode,

$$\tau_{ri}(t) = \frac{-m_i R_i}{q h_i(t)} \Bigg[K_{si} |S_i(t)|^{\chi} \text{sign}(S_i(t)) - q(v_{i-1}(t) - v_i(t)) - q\kappa e_i(t) + \dot{e}_{i+1}(t) + \kappa e_{i+1}(t) + q h_i(t) \Big[\frac{-1}{m_i R_i} \big(I_{fi} \dot{\omega}_{fi}(t) + I_{ri} \dot{\omega}_{ri}(t) \big) - \frac{F_{Ri}(t)}{m_i} \Big] \Bigg], \quad i = 1, ..., N-1, \tag{20}$$

and, for the N^{th} vehicle,

$$\tau_{rN}(t) = \frac{-m_i R_i}{q h_i(t)} \Bigg[K_{si} |S_i(t)|^{\chi} \text{sign}(S_i(t)) - q(v_{i-1}(t) - v_i(t)) - q\kappa e_i(t) + q h_i(t) \Big[\frac{-1}{m_i R_i} \big(I_{fi} \dot{\omega}_{fi}(t) + I_{ri} \dot{\omega}_{ri}(t) \big) - \frac{F_{Ri}(t)}{m_i} \Big] \Bigg]. \tag{21}$$

Similar expressions are derived for braking. The string stability conditions and Lyapunov stability in the presence of external disturbances using PRERL has been established in [9].

V. Adaptive Time-headway Policy

Simulations were conducted using the presented platoon framework to understand the relationship between energy consumption, time-headway, and vehicle operating speed. The complete vehicle dynamics model presented in Section II integrated with the SMC presented in Section IV to track different speed profiles and ensure stable operation. Multiple factors, viz., operating speed, road slope, acceleration/braking maneuvers, loading conditions, tyre-road friction coefficient, etc., influence the energy consumed per operation. The model presented in Section III is used to compute the energy consumption for travelling a distance of 1 km at a constant speed. A map presenting energy consumption as a function of $h_i(t)$ and $v_i(t)$ was generated ($\mathcal{E}_{Ci}(h_i(t), v_i(t))$) and is presented in Fig. 2. Energy consumption for a fully laden individual truck in the platoon operating on a straight and level dry road ($\theta = 0$, $\mu = 0.8$) is presented. The plot is generated for different $h_i(t)$ magnitudes and different operating speeds ranging from 50-70 km/h at which previous studies have shown lower energy consumption [16]. Time simulations have been done for the aforementioned operating conditions, and a map is generated relating energy consumption, operating speed, and time-headway.

From Fig. 2, the energy consumption increases considerably as time-headway magnitude increases. As $h_i(t)$ increases (for a constant speed), the intervehicular spacing increases, thus increasing the aerodynamic drag. However, interestingly, the energy consumption does not increase after a particular threshold value of $h_i(t)$ (in this work, the value was found to be 15 s). This is because, after a particular value of $h_i(t)$, the vehicles can no longer considered to be in a platoon formation, and the energy consumption magnitudes approach that of a vehicle operating independently. In such a scenario, the aerodynamic drag reduction would no longer be applicable ($C_{D_i} = C_{D_0}$). The energy consumption also increases as speed increases.

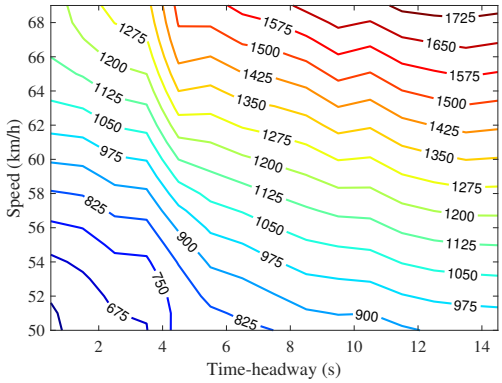

Fig. 2: Map showing energy consumption as a function of time-headway and longitudinal speed.

This map can be used as a guide for selecting different speed and headway magnitudes for the desired energy consumption or vice versa. If one were to impose a constraint on the total energy consumed for each vehicle during a particular route (or in terms of distance), then it is possible to choose a convenient $h_i(t)$ and operating speed from Fig. 2. For instance, from Fig. 2, if there is a requirement to limit the energy consumption to 900 kJ for a distance of 1 km (by choosing the constant energy consumption contour), individual vehicles in the platoon could choose any $(h_i(t), v_i(t))$ value from the corresponding contour. For a platoon travelling at 60 km/h, the magnitude of $h_i(t)$ should be kept at 0.5 s to limit the energy consumption to 900 kJ. Due to operating constraints, if it is required to increase the headway magnitude to 5 s, then to maintain the energy consumption at the same value, the platoon speed has to be reduced to 55 km/h (by following the 900 kJ contour).

VI. Energy Consumption Map Considering Deceleration Demand

It is critical to consider the effect of changing $h_i(t)$ and $v_i(t)$ magnitudes on platoon stability during perturbation maneuvers. On a highway, for a vehicle cruising at a particular speed, one of the most crucial factors that can cause collisions is the sudden application of brakes. In this regard, the platoon stability is analysed by applying brakes (to introduce lead vehicle speed perturbations) at different deceleration and time-headway magnitudes.

The minimum time-headway ($h_{i_{min}}$) required to have a stable platoon for different speeds is obtained for different deceleration magnitudes using the vehicle dynamics-based platoon and controller frameworks presented in Sections II and IV, respectively. If the platoon is forced to operate below $h_{i_{min}}$ at a particular speed, and if there a perturbation in the leader speed profile (by braking), then the follower vehicles could collide each other and result in string instability. For instance, for deceleration values of 1 m/s^2, 2 m/s^2, and 3

m/s^2, $h_{i_{min}}$ required for a platoon operating at 60 km/h are 0.5 s, 1 s, and 2 s, respectively. Lowering the headway magnitude below $h_{i_{min}}$ for reducing energy consumption would result in vehicle collisions. This would mean that the energy consumption map presented in Fig. 2 should also be updated incorporating the same.

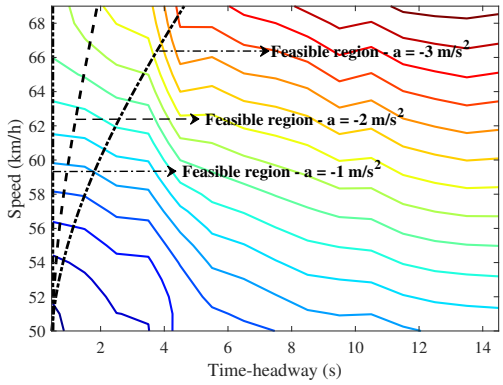

Fig. 3: Updated energy consumption map showing feasible regions for different deceleration values. Feasible region is towards the right of $h_{i_{min}}$ contours.

Figure 3 presents the updated $\mathcal{E}_{Ci}(h_i(t), v_i(t))$ map incorporating $h_{i_{min}}$ constraint for different deceleration values. This map represents the minimum attainable energy consumption magnitude at each speed. The feasible region of operation lies to the right of the $h_{i_{min}}$ curves. It is possible to keep vehicles closer for lower deceleration magnitudes, thus reducing energy consumption even at higher speeds. However, in high deceleration scenarios (such as panic braking situations), the vehicles should keep a higher minimum safe distance between themselves to prevent collisions. To limit the energy consumption to 900 kJ as in the previous case for a vehicle travelling at 60 km/h, the headway magnitude should be kept at least 0.5 s, which would limit the deceleration to 1 m/s^2. For higher deceleration values, the $h_{i_{min}}$ magnitudes (from Fig. 3) are higher than 0.5 s, and this would result in increased energy consumption compared to that of the desired value. Nevertheless, this trade-off will ensure platoon stability and reduce the total energy consumption compared to that of constant headway scenarios.

Remark 1: The analysis and the plots are presented for only one specific operating condition. A straight and level dry road ($\theta = 0$, $\mu = 0.8$) for a distance of 1 km is used to generate the plots presented above. Using the presented platoon framework, similar plots have been obtained for different road lengths, slopes, and road types (wet, dry, based on μ values), with some quantitative changes.

VII. Results and Discussions

To test the efficacy of the proposed adaptive time-headway policy, a five-vehicle platoon with one leader and four follower trucks has been considered. Each follower vehicle is realised using the vehicle parameters as in [9], assuming a homogeneous platoon. The complete vehicle dynamics model with adaptive time-headway policy and the string stable controller have been programmed in MATLAB SIMULINK®.

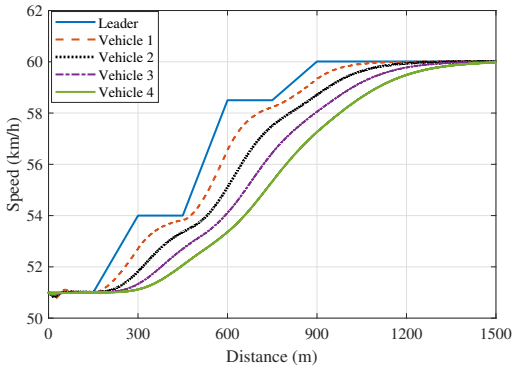

Fig. 4: Speed tracking profiles.

The follower vehicles in the platoon are made to track an accelerating leader speed profile using the proposed adaptive time-headway policy. A time-varying speed profile is chosen to check the efficacy of the proposed approach. The desired total energy consumption magnitude (obtained from the steady state $\mathcal{E}_{Ci}(h_i(t), v_i(t))$ map) at the end of 1.5 km was fixed to be 1300 kJ. The speed tracking profiles are presented in Fig. 4. The initial non-minimum phase characteristics shown in the speed tracking profile are due to actuator delays in the system. The speed tracking is repeated for a constant $h_i(t)$ magnitude, and imposing the constraints of different deceleration demands. In all the cases, similar tracking profiles (as in Fig. 4) were observed. The corresponding time-headway profiles are presented in Fig. 5.

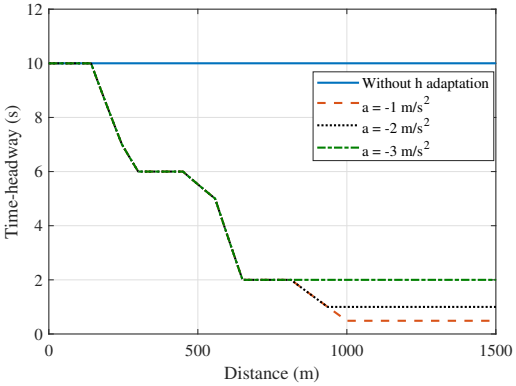

Fig. 5: Time-headway variation for keeping desired energy consumption.

Headway profiles with and without the proposed approach are presented. Using the proposed approach, the headway magnitude varies adaptively according to the changes in the speed profile to maintain the desired energy consumption.

Headway profiles incorporating deceleration demand constraints are also presented. For instance, for $a = -3$ m/s^2, the lower bound for headway magnitude is 2 s even though it is desired to keep it at $h_i(t) = 0.5$ s, and hence increasing the energy consumption. The energy consumption profiles for the headway variations in Fig. 5 is presented in Fig. 6.

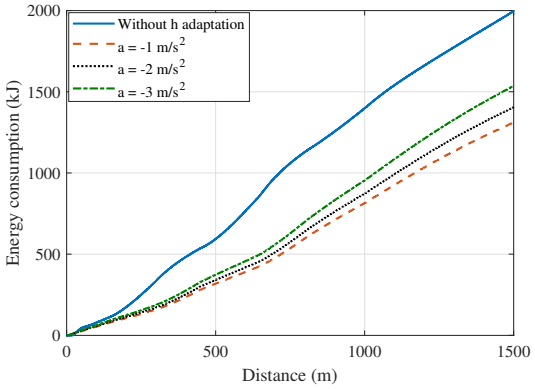

Fig. 6: Plots showing reduction in energy consumption using the proposed time-headway adaptation.

Without the proposed adaptive time-headway policy, the total energy consumption at the end of 1.5 km was $\approx$ 2000 kJ. When there are no constraints imposed/at low deceleration magnitudes, at the end of 1.5 km, the total energy consumption is 1305 kJ (desired value was 1300 kJ). Using the proposed approach, there was a 34.75% reduction in total energy consumption compared to the conventional method of keeping $h_i(t)$ constant. Even after incorporating headway magnitude bounds according to deceleration demands, the proposed approach has considerable fuel savings, as presented in Fig. 6. Even after applying the headway bounds, the proposed policy is found to be having 29.73% and 22.9% energy consumption reduction for deceleration values of 2 m/s^2 and 3 m/s^2, respectively, compared to the constant h_i approach.

VIII. Conclusions

An adaptive time-headway policy for reducing the energy consumption of truck platoons has been presented. A nonlinear framework incorporating multiple critical factors to emulate on-road platoon operations has been used to generate a map between energy consumption, time-headway and operating speed. Rather than keeping a constant time-headway value, the systematic approach presented could adjust the headway magnitude to suit the energy consumption requirements according to different operating speeds and deceleration demands. The map data could be used by fleet operators to formulate policy decisions such as managing the total energy consumption for a particular route by choosing drive cycle/headway according to the operating conditions. Alternatively, it is also possible to predict how much fuel is needed for a particular route for different headway profiles and operating speed. This would help in devising efficient and economical fleet management strategies. The proposed approach can also be suitably modified for the range prediction for electric vehicle/electric vehicle platoons. Additional factors like state of charge could be included in the framework, which could be the future direction of this work.

Acknowledgements

The authors thank the Ministry of Skill Development and Entrepreneurship, Government of India, for funding through the grant EDD/14-15/023/MOLE/NILE. The third author acknowledges the partial funding support from the CFCM industrial contracts and the TSB CMDC/10005693.

References

[1] S. Sivanandham and M. Gajanand, "Platooning for sustainable freight transportation: an adoptable practice in the near future?" *Transport Reviews*, pp. 1–26, 2020.

[2] A. Alam, B. Besselink, V. Turri, J. Mårtensson, and K. H. Johansson, "Heavy-duty vehicle platooning for sustainable freight transportation: A cooperative method to enhance safety and efficiency," *IEEE Control Systems Magazine*, vol. 35, no. 6, pp. 34–56, 2015.

[3] K.-Y. Liang, J. Mårtensson, and K. H. Johansson, "Heavy-duty vehicle platoon formation for fuel efficiency," *IEEE Transactions on Intelligent Transportation Systems*, vol. 17, no. 4, pp. 1051–1061, 2015.

[4] V. Turri, B. Besselink, and K. H. Johansson, "Cooperative look-ahead control for fuel-efficient and safe heavy-duty vehicle platooning," *IEEE Transactions on Control Systems Technology*, vol. 25, no. 1, pp. 12–28, 2016.

[5] S. W. Smith, Y. Kim, J. Guanetti, R. Li, R. Firoozi, B. Wootton, A. A. Kurzhanskiy, F. Borrelli, R. Horowitz, and M. Arcak, "Improving urban traffic throughput with vehicle platooning: Theory and experiments," *IEEE Access*, vol. 8, pp. 141 208–141 223, 2020.

[6] D. Swaroop and J. K. Hedrick, "String stability of interconnected systems," *IEEE Transactions on Automatic Control*, vol. 41, no. 3, pp. 349–357, 1996.

[7] Y. Zheng, S. E. Li, J. Wang, D. Cao, and K. Li, "Stability and scalability of homogeneous vehicular platoon: Study on the influence of information flow topologies," *IEEE Transactions on intelligent transportation systems*, vol. 17, no. 1, pp. 14–26, 2015.

[8] X. Guo, J. Wang, F. Liao, and R. S. H. Teo, "Distributed adaptive integrated-sliding-mode controller synthesis for string stability of vehicle platoons," *IEEE Transactions on Intelligent Transportation Systems*, vol. 17, no. 9, pp. 2419–2429, 2016.

[9] K. B. Devika, G. Rohith, V. R. S. Yellapantula, and S. C. Subramanian, "A dynamics-based adaptive string stable controller for connected heavy road vehicle platoon safety," *IEEE Access*, vol. 8, pp. 209 886–209 903, 2020.

[10] R. Rajamani, *Vehicle dynamics and control*. Springer Science & Business Media, 2011.

[11] H. Pacejka, *Tire and vehicle dynamics*. Elsevier, 2005.

[12] N. Sridhar, K. V. Subramaniyam, S. C. Subramanian, G. Vivekanandan, and S. Sivaram, "Model based control of heavy road vehicle brakes for active safety applications," in *2017 14th IEEE India Council International Conference (INDICON)*. IEEE, 2017, pp. 1–6.

[13] L. Davis, "Stability of adaptive cruise control systems taking account of vehicle response time and delay," *Physics Letters A*, vol. 376, no. 40-41, pp. 2658–2662, 2012.

[14] A. A. Hussein and H. A. Rakha, "Vehicle platooning impact on drag coefficients and energy/fuel saving implications," *arXiv preprint arXiv:2001.00560*, 2020.

[15] K. B. Devika and S. Thomas, "Power rate exponential reaching law for enhanced performance of sliding mode control," *International Journal of Control, Automation and Systems*, vol. 15, no. 6, pp. 2636–2645, 2017.

[16] M. K. Nasir, R. Md Noor, M. Kalam, and B. Masum, "Reduction of fuel consumption and exhaust pollutant using intelligent transport systems," *The Scientific World Journal*, vol. 2014, 2014.